MULTIPLE SCLEROSIS JOURNAL | MSJ

Original Research Paper

Reliability of paramagnetic rim lesion detection at 1.5T MRI in multiple sclerosis patients

Maria Sofia Martire, Lucia Moiola, Pietro Maggi, Serena Borrelli, Valentina Novati, Vittorio Martinelli, Maria A Rocca, Paolo Vezzulli, Andrea Falini, Massimo Filippi* and Martina Absinta*

Multiple Sclerosis Journal

1–9

DOI: 10.1177/13524585251314358

Abstract

Background: Paramagnetic rim lesions (PRL) are valuable for diagnosing and prognosing multiple sclerosis (MS) and detectable at 7T and 3T MRI. For translation into clinical practice, it is essential assessing their visibility on 1.5T clinical scanners.

Objective: To evaluate the reliability of detecting PRL using commercially available susceptibility-weighted imaging (SWI) at 1.5 versus 3T MRI.

Methods: SWI images were obtained in 20 people with MS at 1.5T and 3T MRI, with an average scan interval of 1.1 years. Only stable, non-enhancing lesions visible on both scans were analyzed. PRL at 3T were identified by two expert raters using NAIMS PRL criteria and used as a reference. Four raters, blinded to 3T results, assessed PRL at 1.5T. Discrepancies were resolved by consensus.

Results: PRL were identified in 16 of 20 patients. At 3T, 95 PRL were identified by consensus (mean 5 PRL per patient, range 0–30). Blinded to 3T scans, 82% of PRL were visible at 1.5T (78 of 95 PRL). Inter-rater reliability was "almost perfect" for both 1.5 and 3T scans. Raters accurately classified all patients as having ⩾1PRL or not at 1.5T.

Conclusion: The majority of PRL are detectable at 1.5T without significantly reducing the specificity of PRL identification or increasing the detection of pseudo-PRL. This may facilitate their clinical use in MS diagnosis and prognosis.

Keywords: Multiple sclerosis, paramagnetic rim lesions, diagnosis, susceptibility-based MRI

Date received: 13 November 2024; revised: 20 December 2024; accepted: 3 January 2025

Correspondence to:
M Absinta
IRCCS San Raffaele Scientific Institute, Via Olgettina 60, 20132, Milan, Italy.
martina.absinta@hunimed.eu

Maria Sofia Martire
Neurology Unit, IRCCS San Raffaele Hospital, Milan, Italy; Vita-Salute San Raffaele University, Milan, Italy; Translational Neuropathology Unit, Division of Neuroscience, IRCCS San Raffaele Scientific Institute, Milan, Italy

Lucia Moiola
Vittorio Martinelli
Neurology Unit, IRCCS San Raffaele Hospital, Milan, Italy

Pietro Maggi
Serena Borrelli
Neuroinflammation Imaging Lab (NIL), Institute of NeuroScience, Université Catholique de Louvain, Brussels, Belgium; Department of Neurology, Hôpital Erasme, Hôpital Universitaire de Bruxelles, Université Libre de Brussels, Brussels, Belgium

Valentina Novati
Paolo Vezzulli
Neuroradiology Unit, IRCCS San Raffaele Hospital, Milan, Italy

Maria A Rocca
Massimo Filippi
Neurology Unit, IRCCS San Raffaele Hospital, Milan, Italy; Vita-Salute San Raffaele University, Milan, Italy; Neuroimaging Research Unit, Division of Neuroscience, IRCCS San Raffaele Scientific Institute, Milan, Italy

Andrea Falini
Vita-Salute San Raffaele University, Milan, Italy; Neuroradiology Unit, IRCCS San Raffaele Hospital, Milan, Italy

Introduction

Multiple sclerosis (MS) is a chronic inflammatory and neurodegenerative disease of the central nervous system, where timely diagnosis and early initiation of disease-modifying treatments are crucial for favorable clinical outcomes.[1] To enhance the specificity of McDonald 2017 MS criteria,[2] novel magnetic resonance imaging (MRI) biomarkers have been recently explored.[3] Among those, paramagnetic rim lesions (PRL)[4] have shown high diagnostic specificity for MS in multicenter studies,[5–8] improving accuracy when combined with existing criteria or with other imaging biomarkers, including the central vein sign (CVS) and cortical lesions.[5,8–10] In the recently presented revised McDonald criteria,[11] PRL are set to be introduced into clinical practice, in certain situations, as an additional paraclinical feature, thereby enhancing diagnostic specificity and reducing time to MS diagnosis.

PRL are also predictive of disease severity and disability progression independent of clinical relapses (PIRA),[12–17] as they reflect compartmentalized chronic inflammation in MS—a process currently lacking of effective treatments.[18] For this reason, PRL are being explored as outcome measures in clinical trials [e.g. NCT04025554, NCT04742400, NCT03222973, NCT03523858], with experts anticipating their use in clinical practice to guide treatment decisions.

Martina Absinta
Translational Neuropathology Unit, Division of Neuroscience, IRCCS San Raffaele Scientific Institute, Milan, Italy; Department of Biomedical Sciences, Humanitas University, Milan, Italy.

*Massimo Filippi and Martina Absinta shared equal contribution.

However, the widespread implementation of PRL detection is hindered by limited access to high-field MRI (3T or 7T), uncertainties regarding optimal MRI protocols, and the need for standardized PRL identification and rater agreement. The recent NAIMS consensus[19] provides detailed guidelines for PRL assessment and reporting on MRI. While PRLs can be visualized at 7T and 3T,[20] and even at 1.5T MRI,[21] comparative studies using the PRL NAIMS criteria[19] across different field strengths are lacking. Prior research has confirmed the comparability of 7T and 3T MRI for PRL detection,[20] enabling their use in multicenter studies and trials. Nevertheless, it is essential to assess PRL visibility on the more commonly available 1.5T MR scanners before their widespread adoption in daily clinical practice.

This study aimed to evaluate the reliability of detecting PRLs at 1.5T versus 3T MRI using susceptibility-weighted imaging in a cohort of 20 people living with MS.

Materials and methods

Participants

From March 2022 to June 2024, we prospectively recruited for 3T MR imaging 20 adult people living with MS (mean age 41 years, range 23–58; female 68%) that were under regular clinical and radiological follow-up at the Multiple Sclerosis Center, IRCCS San Raffaele Hospital in Milan (Italy). Seventeen patients had a relapsing-remitting, while three had a progressive course of disease. MS diagnosis was made by expert neurologists according to McDonald Criteria 2017.[2] Median EDSS score was 2.0 (range 0–5.0) and average disease duration was 9 years (range 0.5–24 years). After enrollment, a retrospective evaluation of 1.5T MRI images acquired for clinical purposes, and closest to the 3T MRI acquisition, was performed for all patients. Imaging and clinical data were collected under institutional review board-approved protocols. Demographic and clinical data are fully detailed in Table 1.

MR imaging acquisition

Participants underwent two MR imaging acquisitions, one on a Philips Ingenia Ambition X 1.5T MR imaging scanner (equipped with a 16-channel head coil) and one on Philips Ingenia 3T CX MR imaging scanner (equipped with a 32-channel head coil). The order of acquisition was random, with the first acquisition being performed on the 1.5T MR scanner in 15 out of 20 patients. On average, the time lapse between scans was 1.1 years (median 0.7 years, range 4 days to 4.5 years).

The 3T MR imaging protocol included:

- Whole-brain 3D T2 FLAIR (TR = 4800 ms; TE = 373 ms; acquisition time = 5:50 minutes; number of sagittal slices: 180; acquisition voxel size: $1 \times 1 \times 1\,mm^3$; reconstructed voxel size: $0.94 \times 0.94 \times 1\,mm^3$).
- Whole-brain 3D susceptibility-weighted imaging (SWI) providing T2*-magnitude and unwrapped filtered phase contrasts (TR = 31 ms; TE = 7.2 ms; flip angle = 17°; acquisition time = 6:04 minutes; number of axial slices: 260; acquisition voxel size: $0.6 \times 0.6 \times 1\,mm^3$; reconstruction voxel size: $0.45 \times 0.45 \times 0.5\,mm^3$).

The 1.5T MR imaging protocol included:

- Whole-brain 3D T2 FLAIR (TR = 4800 ms; TE = 295 ms; acquisition time = 5:31 minutes; number of sagittal slices: 321; acquisition voxel size: $1.15 \times 1.15 \times 1.15\,mm^3$; reconstructed voxel size: $1 \times 1 \times 0.57\,mm^3$).
- Whole-brain 3D susceptibility-weighted imaging (SWI) providing T2*-magnitude and unwrapped filtered phase contrasts (TR = 51 ms; TE = 12 ms; flip angle = 20°; acquisition time = 6:06 minutes; number of axial slices: 130; acquisition voxel size: $1 \times 1 \times 2\,mm^3$; reconstructed voxel size: $0.3 \times 0.3 \times 1\,mm^3$).

To replicate real-life radiological assessments, phase image unwrapping and filtering for both 3T and 1.5T SWI images were performed directly on the scanner using the Philips-provided phase reconstruction processing.

Other MRI sequences such as pre-contrast and post-contrast T1 spin-echo (for 1.5T MRI acquisition only) were evaluated to exclude gadolinium enhancing lesions from the study. Pre-contrast 3D T1-weighted MPRAGE sequence were available only for 3T MRI acquisition.

MR imaging analysis

After anonymization, image visualization and analysis implemented MIPAV (https://mipav.cit.nih.gov/), Horos software (https://horosproject.org/) and the institutional radiological viewer XERO (https://xero.ihsr.dom/). To closely simulate real-life radiological assessments typically performed in non-specialized

Table 1. Demographic and clinical characteristics of the cohort (at the time of the first scan).

Subject	Age	Sex	Clinical phenotype	EDSS	Disease duration (years)	Treatment	Time lapse between scans (years)	3T PRL count by consensus
1	23	F	RR	1.5	1	Natalizumab	0.7	3
2	51	F	RR	3.0	6	Untreated	0.4	1
3	40	F	RR	1.5	23	Glatiramer Acetate	0.8	1
4	48	M	SP	3.5	11	Fingolimod	0.7	2
5	53	M	SP	5.0	8	Azathioprine	0.1	3
6	44	F	RR	0	1	Dimethyl Fumarate	0.4	1
7	48	F	RR	1.5	15	Fingolimod	0.3	1
8	58	F	RR	1.5	11	Fingolimod	0.7	0
9	27	F	RR	0	1	Ocrelizumab	1.2	1
10	34	M	RR	1.0	7	Cladribine	4.5	6
11	25	M	RR	3.0	7	untreated (post-HSCT)	2.5	30
12	27	F	RR	1.0	5	Ofatumumab	0.2	0
13	58	M	SP	3.0	3	Siponimod	1.5	20
14	34	F	RR	3.0	0.5	Dimethyl fumarate	0.4	0
15	42	F	RR	2.0	20	Dimethyl fumarate	0.1	1
16	48	M	RR	2.5	24	Dimethyl fumarate	0.3	1
17	36	F	RR	1.5	3	Alemtuzumab	3.1	3
18	32	F	RR	1.0	2	Ocrelizumab	1.9	0
19	52	F	RR	1.5	3	Ofatumumab	1.8	21
20[a]	39	F	RR	1.0	1.5	Natalizumab	1.5	2

RR: relapsing MS; SP: secondary progressive MS; HSCT: hematopoietic stem cell transplantation.
[a]Case excluded due to motion artifacts in one scan.

centers, we analyzed SWI-phase images directly processed by the MRI scanner and assessed white matter lesions on T2-FLAIR and SWI-phase images plane by plane. According to NAIMS PRL consensus criteria,[19] we classified a white matter lesion as PRL when having the following imaging features:

-A discrete rim with paramagnetic properties on susceptibility-weighted MRI sequence that is continuous through at least 2/3 of the outer edge of the WM portion of the lesion.
-The rim colocalizes with the edge of all or part of a lesion core that is hyperintense on T2-FLAIR images.
-The rim (or part of it) is discernible on two orthogonal planes.

Only non-enhancing lesions visible on both scans were evaluated for PRL identification. Given the lack of standards and recommendations regarding infratentorial PRL, only supratentorial PRL were evaluated in this study. Following the PRL NAIMS criteria,[19] confluent lesions were not excluded from the analysis and the PRL count was based on the clear identification of sublesional areas surrounded by paramagnetic rims.

Overall, the PRL assessment included four raters: three MS-specialized neurologists (M.A., S.B., P.M.) with years of experience in MS imaging, including PRL identification, as well as a resident in neurology (M.S.M.) who underwent a dedicated training of 2 years in PRL identification.

PRL assessment at 3T MRI. For this study, PRL detected on SWI-phase image at 3T MRI were considered the gold-standard for comparison with 1.5T assessment. For each case, two raters (M.A. and M.S.M.) simultaneously analyzed whole-brain T2-FLAIR and SWI-phase images and recorded the presence and location of PRL by consensus.

PRL assessment at 1.5T MRI. Blinded to the 3T MRI, PRL assessment at 1.5T MRI was performed by a total of four raters using two different approaches as follows.

(1) *PRL assessment screening 1.5T whole-brain MR images.* In the first analysis, for each subject, two raters (M.A. and M.S.M.) independently evaluated T2-FLAIR and SWI-phase images, recording the presence and location of PRL. To minimize recall bias, the rating of 1.5T and 3T images was conducted by the two raters with a minimum interval of 6 months between analyses. Interrater agreement was calculated. Disagreements were then resolved by re-analysis of the images, and a final consensus was reached. After consensus, discrepancies between PRL assessment at 1.5T versus 3T (gold standard) were retrospectively investigated and discussed.

(2) *Lesion selection-based 1.5T PRL assessment.* For each subject, five discrete randomly selected chronic supratentorial white matter lesions were marked with an arrow on screenshots of the 1.5T T2-FLAIR and SWI-phase single-slice images and subsequently evaluated by two other independent investigators (P.M. and S.B.). Each lesion was assigned a binary code (0 = no PRL, 1 = PRL). Interrater reliability was calculated. After 1 month, the two raters (P.M. and S.B.) repeated the same evaluation, blinded to their prior results, to assess intrarater reliability. Discrepancies between PRL assessment at 1.5T and 3T (considered the gold standard) were retrospectively investigated and discussed.

Statistical analysis

Interrater and intrarater agreement were computed using Cohen's kappa (κ).

Results

A total of 516 supratentorial MS lesions were identified and assessed for PRL status. Among these lesions, 52% were periventricular, 21% were juxtacortical/leukocortical, and 27% were located in the deep white matter. Two lesions showing gadolinium enhancement on post-contrast T1-weighted images at 1.5T were excluded. The 1.5T images of one patient were excluded for motion artifacts.

PRL assessment at 3T MRI (gold standard of this study)

By consensus agreement, 95 of 516 lesions (18.4%) were identified as PRL on 3T SWI-phase images. Only 39 of 95 PRL (39%) were also visible on SWI-magnitude images.

Of the 95 PRL, 47% were located in periventricular white matter, corresponding to 17% of the total T2-FLAIR lesions in this location. A total of 13% of PRL were located in juxtacortical/leukocortical areas, representing 11% of the total T2-FLAIR lesions in that region. The remaining 40% of PRL were located in the deep white matter/centrum semiovale, accounting for 27% of the total T2-FLAIR lesions in this area; 16 of 20 patients had at least 1 PRL (Table 1). The median number of PRL per patient was 1 (average 5, range 0–30) (Table 1).

PRL assessment screening on whole-brain 1.5T MR images

By consensus agreement, 78 of 516 lesions (14.3%) were judged PRL on 1.5T SWI-phase images (blinded to the 3T MRI results). The interrater reliability was "almost perfect," with a Cohen κ of 0.851 (Table 2). At the patient level, both raters properly classified MS cases as either having no PRL (4 of 19 patients) or at least 1 PRL (15 of 19 patients).

Lesion selection-based 1.5T PRL assessment

Of the 100 selected lesions, 50 were identified as PRL on 1.5T SWI-phase images. The intrarater and interrater agreement results are provided in Table 2. The reliability between each rater and the consensus agreement was rated as perfect/almost perfect, with Cohen κ ranging from 0.97 to 1.00.

Lesion rim assessment at 3T versus 1.5T MRI and analysis of disagreement

At 1.5T MRI, the raters identified 82% (78 out of 95) of the PRL identified at 3T MRI. Examples of PRL at 1.5T and 3T MRI are shown in Figure 1(a) and (b).

Discrepancies between 1.5T and 3T were observed in 17 lesions and were further discussed:

- Four lesions were classified as PRL on 3T MRI but as "nodular" (having homogeneous hypointensity on SWI-phase images) on 1.5T MRI. These "false negative" PRL are likely due to the lower magnetic strength and voxel resolution of the 1.5T SWI images (Figure 2(a)).
- Two lesions were recorded as PRL on 3T MRI but were PRL-negative on 1.5T MRI. This discrepancy is likely due to the lesions' spatial proximity to draining venule-rich regions such as the ventricles, which complicate the visualization of paramagnetic rims (Figure 2(b)).

Table 2. Raters agreement.

	Cohen's κ	Percentage of agreement	Agreement
PRL 3T vs. 1.5T			
3T vs. 1.5T consensus	0.875 (CI 95% = 0.811–0.939)	97%	Almost perfect
PRL assessment screening 1.5T whole-brain MR images (rater 1: msm; rater 2: ma)			
Interrater	0.851 (CI 95% = 0.780–0.923)	96%	Almost perfect
Lesion selection-based 1.5T PRL assessment (rater 1: pm; rater 2: sb)			
Interrater	0.97 (CI 95% = 0.873–1.00)	97%	Almost perfect
Intrarater (rater 1)	0.84 (CI 95% = 0.733–0.946)	92%	Almost perfect
Intrarater (rater 2)	1.00 (CI 95% = 1.00–1.00)	100%	Perfect
Each rater vs consensus (rater 1)	0.97 (CI 95% = 0.873–1.00)	97%	Almost perfect
Each rater vs consensus (rater 2)	1.00 (CI 95% = 1.00–1.00)	100%	Perfect

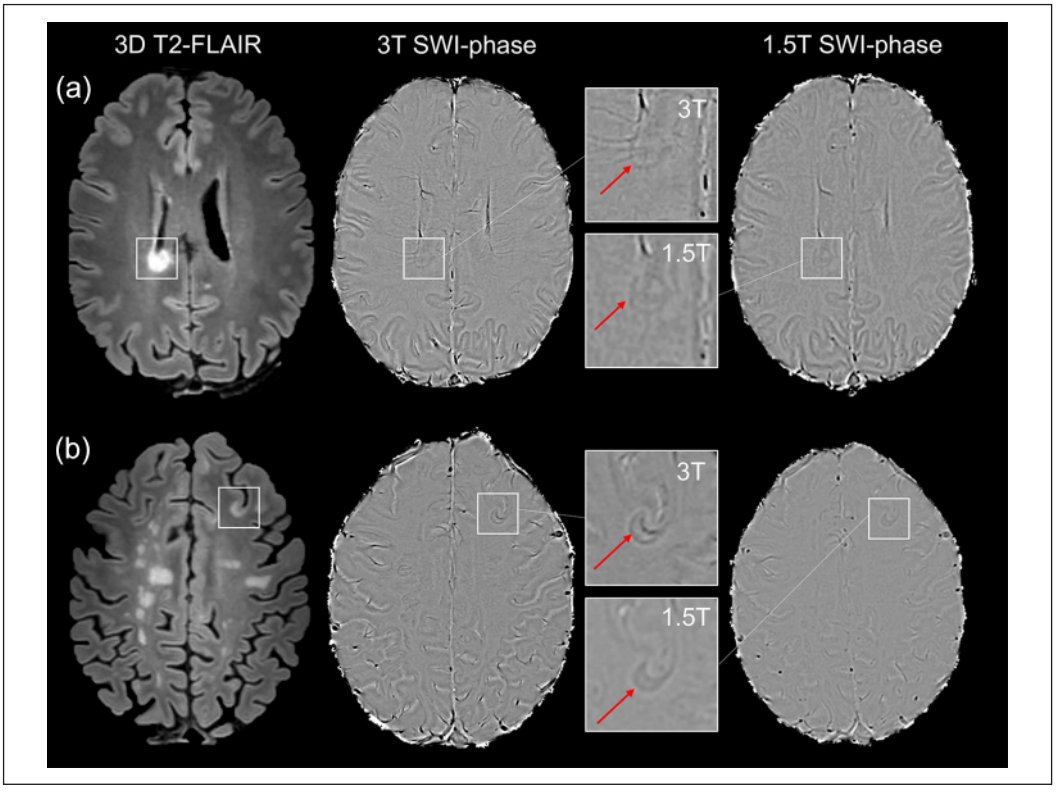

Figure 1. Concordant PRL at 1.5T and 3T MRI. (a) Axial 3D FLAIR and SWI phase images from subject #7 (Table 1) showing a comparable visualization of a periventricular PRL at different magnetic fields. The time lapse between scans was 0.3 years. (b) Axial 3D FLAIR and SWI phase images from subject #11 (Table 1) showing a leukocortical PRL at both 1.5T and 3T. The time lapse between scans was 2.5 years. For both cases, PRL magnification is shown in the insets at both 1.5 and 3T MRI. In both cases, a clear distinction between the hypointense phase rim and the isointense core of the lesion can be noticed.

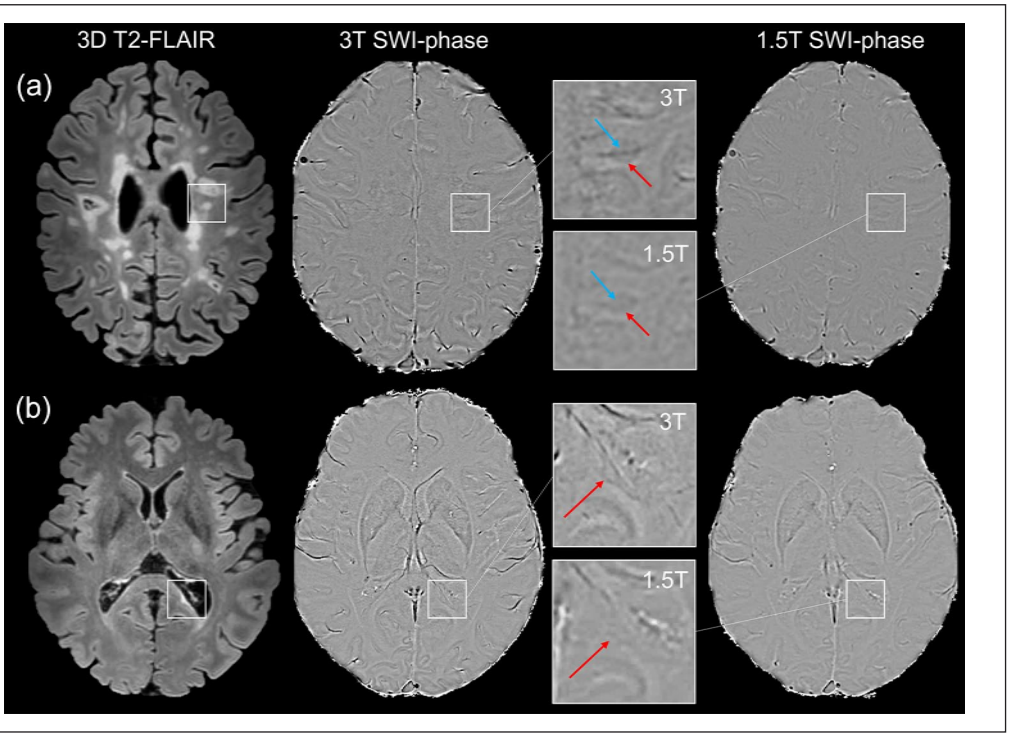

Figure 2. Discordant PRL at 1.5T versus 3T MRI. (a) Axial 3D FLAIR and SWI phase images from subject #11 (Table 1) showing a small white matter lesion (red arrow) classified as PRL at 3T MRI, but as hypointense nodular at 1.5T MRI. The time lapse between scans was 2.5 years. The central vein (blue arrow) is also more visible at 3T. (b) Axial 3D FLAIR and SWI phase images from subject #5 (Table 1). The occipital horn of the lateral ventricle, periventricular draining venules, and the optic radiation make difficult the PRL detection at 1.5T. The time lapse between scans was 0.1 year. For both cases, PRL magnification is shown in the insets at both 1.5 and 3T MRI.

- The remaining 11 lesions identified as PRL on 3T MRI but not on 1.5T MRI, appeared confluent at 1.5T MRI. The higher resolution of 3T MRI enabled the identification of a discrete rim. A representative example of this issue is shown in Figure 3.

Discussion

Imaging biomarkers, such as PRLs and CVS, offer high specificity for MS, as they are rarely found in other CNS diseases that clinically or radiologically mimic MS.[5,6,8,22] The imminent introduction of these biomarkers in the revised MS diagnostic criteria[11] is expected to reinforce diagnostic accuracy. However, the reliability of susceptibility-based sequences available in clinical MRI scanners, as well as the applicability of NAIMS practical guidelines[19] for PRL detection, remain unknown.

In this study, we aimed to standardize the approach and minimize detection bias by applying the NAIMS criteria for PRL identification on both 1.5T and 3T MRI scans. To evaluate the suitability of these criteria across different magnetic field strengths, we employed two methods for comparative PRL analysis. The first method aimed to simulate a "real-world" clinical assessment, in which a whole-brain scan (including T2-FLAIR and SWI-phase images) was provided, and PRL were carefully and actively searched for. The second approach involved providing investigators with preselected and marked lesions for focused lesion rating, which helped reduce potential confounders that could arise in whole-brain scan analysis.

In both analyses, intra- and interrater agreement was nearly perfect, demonstrating the high reliability of PRL detection at 1.5T MRI when raters are trained in their identification. Our results surpassed the performance of previous comparative reliability studies at different magnetic field strengths.[20,21] One possible explanation for this improvement is the application of consensus guidelines, which standardized PRL detection and thus enhanced interrater agreement even at lower magnetic field strengths. In addition, the raters' increased experience in PRL research likely improved their rating accuracy over the past years.

By comparing and discussing 1.5T versus 3T imaging assessments, several relevant observations emerged regarding PRL visualization at lower magnetic field

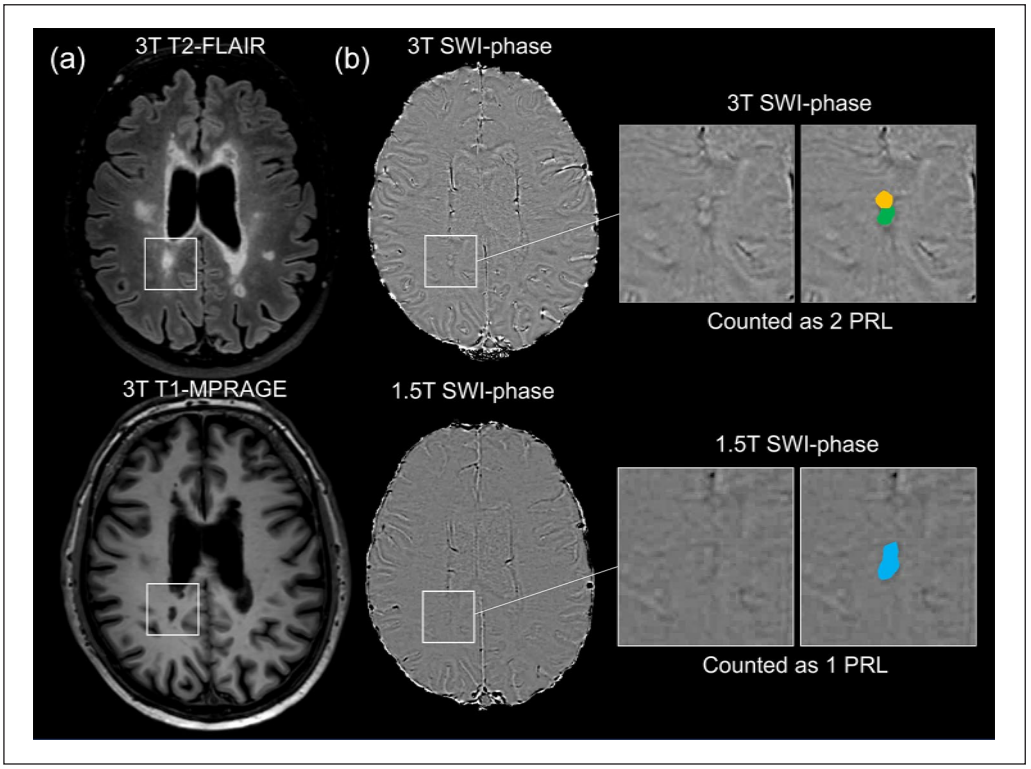

Figure 3. Discordant PRL count at 1.5T versus 3T MRI due to confluent lesions. (a) Axial 3D FLAIR and 3D T1 MPRAGE images from subject #13 (Table 1) show a lesion in the periventricular white matter of the right parietal lobe. (b) On 3T axial SWI-phase images, the paramagnetic rim allows for the identification of two distinct PRLs. In contrast, on 1.5T axial SWI-phase images, the interface between the two lesions appears indistinct, leading to the classification of the lesions as a single PRL. Magnified images are shown in the insets along with the corresponding lesion masks.

strengths: (1) submillimetric in-plane voxel resolution of the SWI-phase image is critical for PRL visualization at any magnetic field strength, including at 1.5T; (2) homogeneously susceptibility-hypointense lesions (referred to as "nodular") can create classification challenges at 1.5T (an example is shown in Figure 2(a)); (3) raters should exercise caution in areas with dense venular vasculature, such as the periventricular regions, as these areas are prone to paramagnetic rim misclassification due to susceptibility artifacts (Figure 2(b)); and (4) confluent lesions, which are common in progressive and older patients, may affect PRL counting, particularly at 1.5T MRI.

These classification issues could lead to false-negative PRL identification. However, the analysis did not reveal any false-positive PRL ratings. In the new revised diagnostic criteria,[11] under certain circumstances, the detection of a single PRL can contribute to increasing the likehood of a diagnosis of MS. Importantly, our results provide reassurance that the introduction of PRL into the revised diagnostic criteria, when applied using 1.5T MRI, will not compromise diagnostic accuracy.

Recent advancements in machine learning (ML) and deep learning (DL) have led to the development of tools for detecting PRL on MRI in a semi- or fully automated manner.[23–26] However, these methods primarily rely on training datasets from 3T MRI, which might limit their applicability in routine clinical practice. Recognizing the reliability of lower magnetic field strengths, such as 1.5T, is essential for developing cost-effective MRI protocols and artificial intelligence (AI)-based automated detection tools that are accessible and practical across a wider range of clinical settings. The implementation of AI methods could not only standardize PRL detection across different centers but also simplify MRI interpretation for both neurologists and neuroradiologists. Furthermore, AI-driven approaches can broaden training cohorts, enhance the detection capabilities of ML/DL models, and improve the accuracy of PRL identification, thereby supporting their integration into routine diagnostic workflows.

A potential limitation of our study is the relatively small number of lesions analyzed, along with the time interval between the 1.5T and 3T MRI scans, which

varied from 4 days to as long as 4.5 years (median time lapse 0.7 years, Table 1). The fading and disappearance of the paramagnetic rim have been observed in a subset of PRLs with longer follow-up periods (7–10 years).[27,28] Therefore, any differences in PRL detection are more likely attributable to the magnetic field strengths and SWI voxel resolution, rather than variability in the lesion dynamics themselves. Furthermore, although this was not the primary focus of our study, it is noteworthy that the two-thirds of the patients in this cohort had PRL, exceeding the prevalence reported in prior studies.[6] A potential explanation is the limited size of our cohort, which does not permit statistical inference of PRL prevalence to the general MS population.

In conclusion, our study demonstrates the high reliability of detecting PRLs on commercially available susceptibility-weighted sequences at 1.5T MRI in MS, with strong interrater and intrarater agreement. The NAIMS criteria for PRL detection are practical and maintain excellent consistency across raters and different magnetic field strengths. Overall, these findings suggest that PRL identification could soon become an integral part of clinical practice, aiding clinicians in both the diagnostic process and the prognostic assessment of the disease.

Data Availability Statement

The dataset used and analyzed during the current study is available from the corresponding author on reasonable request.

Declaration of Conflicting Interests

The author(s) declared the following potential conflicts of interest with respect to the research, authorship, and/or publication of this article: L.M. received compensations for speaking activities and/or for participating to advisory board from Merck, Celgene, Biogen, Sanofi, Novartis, Roche, Alexion, and Amgen. P.M. received consulting honoraria from Sanofi, Biogen, and Merck. S.B. received speaker/consulting honoraria from Sanofi, Roche, Janssen, Merck, and Novartis, and research grants from Roche and Sanofi. V.M. received honoraria for speaking and/or for consultancy and support for travel expenses and participation in congresses from Biogen, Roche, Merck, Novartis, Genzyme. M.A.R. received consulting fees from Biogen, Bristol Myers Squibb, Eli Lilly, Janssen, Roche; and speaker honoraria from AstraZaneca, Biogen, Bristol Myers Squibb, Bromatech, Celgene, Genzyme, Horizon Therapeutics Italy, Merck Serono SpA, Novartis, Roche, Sanofi and Teva. She receives research support from the MS Society of Canada, the Italian Ministry of Health, the Italian Ministry of University and Research, and Fondazione Italiana Sclerosi Multipla. She is Associate Editor for Multiple Sclerosis and Related Disorders. M.F. is Editor-in-Chief of the Journal of Neurology, Associate Editor of Human Brain Mapping, Neurological Sciences, and Radiology; received compensation for consulting services from Alexion, Almirall, Biogen, Merck, Novartis, Roche, Sanofi; speaking activities from Bayer, Biogen, Celgene, Chiesi Italia SpA, Eli Lilly, Genzyme, Janssen, Merck-Serono, Neopharmed Gentili, Novartis, Novo Nordisk, Roche, Sanofi, Takeda, and TEVA; participation in Advisory Boards for Alexion, Biogen, Bristol-Myers Squibb, Merck, Novartis, Roche, Sanofi, Sanofi-Aventis, Sanofi-Genzyme, Takeda; scientific direction of educational events for Biogen, Merck, Roche, Celgene, Bristol-Myers Squibb, Lilly, Novartis, Sanofi-Genzyme; he receives research support from Biogen Idec, Merck-Serono, Novartis, Roche, the Italian Ministry of Health, the Italian Ministry of University and Research, and Fondazione Italiana Sclerosi Multipla. M.A. received speaker and/or consulting honoraria from Biogen, Sanofi, Abata Therapeutics, GSK and Immunic Therapeutics. The other authors have no disclosures.

Funding

The author(s) disclosed receipt of the following financial support for the research, authorship, and/or publication of this article: Fondazione Regionale Ricerca Biomedica (FRRB) Early Career Award (1750327), and FISM—Fondazione Italiana Sclerosi Multipla (2023/R-Single/015) co-financed with the "5 per mille" public funding.

ORCID iDs

Maria Sofia Martire https://orcid.org/0009-0007-7479-2695
Lucia Moiola https://orcid.org/0000-0001-6313-4952
Pietro Maggi https://orcid.org/0000-0003-1697-5585
Serena Borrelli https://orcid.org/0000-0002-3186-1562
Maria A Rocca https://orcid.org/0000-0003-2358-4320
Massimo Filippi https://orcid.org/0000-0002-5485-0479
Martina Absinta https://orcid.org/0000-0003-0276-383X

References

1. Brown JWL, Coles A, Horakova D, et al. Association of initial disease-modifying therapy with later

conversion to secondary progressive multiple sclerosis. *JAMA* 2019; 321: 175–187.

2. Thompson AJ, Banwell BL, Barkhof F, et al. Diagnosis of multiple sclerosis: 2017 revisions of the McDonald criteria. *Lancet Neurol* 2018; 17: 162–173.
3. Maggi P and Absinta M. Emerging MRI biomarkers for the diagnosis of multiple sclerosis. *Mult Scler* 2024; 30(14): 1704–1713.
4. Absinta M, Sati P and Reich DS. Advanced MRI and staging of multiple sclerosis lesions. *Nat Rev Neurol* 2016; 12(6): 358–368.
5. Maggi P, Sati P, Nair G, et al. Paramagnetic rim lesions are specific to multiple sclerosis: An international multicenter 3T MRI study. *Ann Neurol* 2020; 88(5): 1034–1042.
6. Martire MS, Moiola L, Rocca MA, et al. What is the potential of paramagnetic rim lesions as diagnostic indicators in multiple sclerosis. *Expert Rev Neurother* 2022; 22(10): 829–837.
7. Meaton I, Altokhis A, Allen CM, et al. Paramagnetic rims are a promising diagnostic imaging biomarker in multiple sclerosis. *Mult Scler* 2022; 28(14): 2212–2220.
8. Borrelli S, Martire MS, Stölting A, et al. Central vein sign, cortical lesions, and paramagnetic rim lesions for the diagnostic and prognostic workup of multiple sclerosis. *Neurol Neuroimmunol Neuroinflamm* 2024; 11(4): e200253.
9. Clarke MA, Cheek R, Kazimuddin HF, et al. Paramagnetic rim lesions and the central vein sign: Characterizing multiple sclerosis imaging markers. *J Neuroimaging* 2024; 34(1): 86–94.
10. Cagol A, Cortese R, Barakovic M, et al. Diagnostic performance of cortical lesions and the central vein sign in multiple sclerosis. *JAMA Neurol* 2024; 81: 143–153.
11. Montalban X. Revised McDonald criteria 2023. In: *ECTRIMS annual meeting 2024*, Copenhagen, 18 September 2024.
12. Absinta M, Sati P, Schindler M, et al. Persistent 7-tesla phase rim predicts poor outcome in new multiple sclerosis patient lesions. *J Clin Invest* 2016; 126: 2597–2609.
13. Absinta M, Sati P, Masuzzo F, et al. Association of chronic active multiple sclerosis lesions with disability in vivo. *JAMA Neurol* 2019; 76: 1520.
14. Absinta M, Lassmann H and Trapp BD. Mechanisms underlying progression in multiple sclerosis. *Curr Opin Neurol* 2020; 33: 277–285.
15. Treaba CA, Conti A, Klawiter EC, et al. Cortical and phase rim lesions on 7 T MRI as markers of multiple sclerosis disease progression. *Brain Commun* 2021; 3(3): fcab134.
16. Altokhis AI, Hibbert AM, Allen CM, et al. Longitudinal clinical study of patients with iron rim lesions in multiple sclerosis. *Mult Scler* 2022; 28(14): 2202–2211.
17. Cagol A, Benkert P, Melie-Garcia L, et al. Association of spinal cord atrophy and brain paramagnetic rim lesions with progression independent of relapse activity in people with MS. *Neurology* 2024; 102: e207768.
18. Maggi P, Vanden Bulcke C, Pedrini E, et al. B cell depletion therapy does not resolve chronic active multiple sclerosis lesions. *EBioMedicine* 2023; 94: 104701.
19. Bagnato F, Sati P, Hemond CC, et al. Imaging chronic active lesions in multiple sclerosis: A consensus statement. *Brain* 2024; 147: 2913–2933.
20. Absinta M, Sati P, Fechner A, et al. Identification of chronic active multiple sclerosis lesions on 3T MRI. *AJNR Am J Neuroradiol* 2018; 39(7): 1233–1238.
21. Hemond CC, Reich DS and Dundamadappa SK. Paramagnetic rim lesions in multiple sclerosis: Comparison of visualization at 1.5-T and 3-T MRI. *AJR Am J Roentgenol* 2022; 219(1): 120–131.
22. Sati P, Oh J, Constable RT, et al. The central vein sign and its clinical evaluation for the diagnosis of multiple sclerosis: A consensus statement from the North American Imaging in Multiple Sclerosis Cooperative. *Nat Rev Neurol* 2016; 12(12): 714–722.
23. Barquero G, La Rosa F, Kebiri H, et al. RimNet: A deep 3D multimodal MRI architecture for paramagnetic rim lesion assessment in multiple sclerosis. *NeuroImage Clin* 2020; 28: 102412.
24. Lou C, Sati P, Absinta M, et al. Fully automated detection of paramagnetic rims in multiple sclerosis lesions on 3T susceptibility-based MR imaging. *NeuroImage Clin* 2021; 32: 102796.
25. Zhang H, Nguyen TD, Zhang J, et al. QSMRim-Net: Imbalance-aware learning for identification of chronic active multiple sclerosis lesions on quantitative susceptibility maps. *NeuroImage Clin* 2022; 34: 102979.
26. La Rosa F, Wynen M, Al-Louzi O, et al. Cortical lesions, central vein sign, and paramagnetic rim lesions in multiple sclerosis: Emerging machine learning techniques and future avenues. *NeuroImage Clin* 2022; 36: 103205.
27. Absinta M, Maric D, Gharagozloo M, et al. A lymphocyte–microglia–astrocyte axis in chronic active multiple sclerosis. *Nature* 2021; 597(7878): 709–714.
28. Dal-Bianco A, Grabner G, Kronnerwetter C, et al. Long-term evolution of multiple sclerosis iron rim lesions in 7 T MRI. *Brain* 2021; 144(3): 833–847.